Computer Modeling in Engineering & Sciences
DOI:10.32604/cmes.2020.010936
Article

Interpolating Isogeometric Boundary Node Method and Isogeometric Boundary Element Method Based on Parameter Space

Hongyin Yang[1,2], Jiwei Zhong[1,*], Ying Wang[3], Xingquan Chen[2] and Xiaoya Bian[2]

[1]State Key Laboratory for Health and Safety of Bridge Structures, Wuhan, 430034, China
[2]School of Civil Engineering and Architecture, Wuhan Institute of Technology, Wuhan, 430074, China
[3]Wuhan Airport Economic Zone Construction Investment and Development Group Co., Ltd., Wuhan, 430000, China
[*]Corresponding Author: Jiwei Zhong. Email: 105031349@qq.com
Received: 08 April 2020; Accepted: 09 June 2020

Abstract: In this paper, general interpolating isogeometric boundary node method (IIBNM) and isogeometric boundary element method (IBEM) based on parameter space are proposed for 2D elasticity problems. In both methods, the integral cells and elements are defined in parameter space, which can reproduce the geometry exactly at all the stages. In IIBNM, the improved interpolating moving least-square method (IIMLS) is applied for field approximation and the shape functions have the delta function property. The Lagrangian basis functions are used for field approximation in IBEM. Thus, the boundary conditions can be imposed directly in both methods. The shape functions are defined in 1D parameter space and no curve length needs to be computed. Besides, most methods for the treatment of the singular integrals in the boundary element method can be applied in IIBNM and IBEM directly. Numerical examples have demonstrated the accuracy of the proposed methods.

Keywords: Interpolating isogeometric boundary node method; isogeometric boundary element method; parameter space; improved interpolating moving least-square method; Lagrangian basis functions

1 Introduction

Isogeometric analysis (IGA) [1,2] has been applied in many areas and it has at least two advantages compared with the traditional methods: (i) the geometry of the model keeps unchanged in the whole procedure; (ii) the refinement can be performed easily in parameter space. Actually, IGA tries to do the analysis directly on the CAD model, in which the solid can be characterized by the boundary with parametric functions [3]. Thus, combining the IGA with the boundary element method (BEM) [4–9] is a natural idea and relative investigations for IGA BEM can be found in [10–13]. In most types of IGA BEM, B-spline and NURBS basis functions are applied. However, some regular geometry can be construed by simple analytical parametric functions, such as circle and sphere. Besides, the parametric function for a curve or surface is not uniform and different CAD packages may use different functions. Is there any possibility to construct an isogeometric method that is independent of parametric functions? One of the most possible method is the boundary face method (BFM) [14]. In BFM [15,16], only the

forms of parametric functions are needed to be known. Actually, the translations between parameter coordinates and physical coordinates can be done easily by functions in some CAD packages [17–20].

In this paper, the idea is applied in an interpolating boundary node method (IBNM), or can also be called an interpolating boundary element-free method (IBEFM) [21–23]. In the original boundary node method (BNM) [24] or Galerkin BNM [25,26] the moving least-square (MLS) approximation [27–30] is used for field approximation, which leads to difficulty for applying boundary conditions. The interpolating moving least-square (IMLS) method [27] with singular weight functions can be implemented to obtain shape function with delta function property. However, it may lead to difficulties while implementation because of the singular weight functions. An improved interpolating moving least-square (IIMLS) approximation was further presented [21,31] with no singular weight functions and has been applied in BEFM [32]. Wang et al. [33] proposed regularized improved interpolating moving least-square method and adaptive orthogonal improved interpolating moving least-square method [34] to avoid the singular moment matrix while computing the shape function.

In this paper, an interpolating isogeometric boundary node method (IIBNM) is proposed. The method can be considered as a general isogeometric method based on parameter space. The parametric functions are only used to characterize the boundary and the IIMLS method is implemented to interpolate the fields, including the displacement and traction fields. An isogeometric boundary element method (IBEM) can also be obtained if the Lagrangian basis functions are implemented to interpolate the fields. In both methods, there is no discretization error and the integrals are performed on isogeometric cells or elements. Besides, the boundary conditions can be applied easily in both methods, since the shape functions obtained by the IIMLS method and Lagrangian basis functions have the interpolating property. Compared with the conventional BEM and BNM, the proposed methods can avoid the discretization error of geometry and can be integrated with Computer-Aided Design (CAD) easily. Compared with BNM and the isogeometric BEMs [10,35,36], the shape functions for field approximation have interpolating property, and it leads to a simpler way to impose the boundary conditions.

2 The Boundary Integral Equation with Isogeometric Cells

In this section, the boundary integral equation (BIE) for 2D elasticity problems is reviewed and discretized by isogeometric cells. The basic equations can be written as

$$\sigma_{ij,j} = 0 \tag{1}$$

$$\varepsilon_{ij} = \frac{1}{2}(u_{i,j} + u_{j,i}) \tag{2}$$

$$\sigma_{ij} = C_{ijkl}\varepsilon_{kl} \tag{3}$$

with

$$C_{ijkl} = \lambda\delta_{ij}\delta_{kl} + \mu(\delta_{ik}\delta_{jl} + \delta_{il}\delta_{jk}) \tag{4}$$

where σ_{ij} are the stresses, ε_{ij} are the strains and u_i are the displacements. C_{ijkl} are the components of the elastic tensor and δ_{ij} are the Kronecker-delta functions. μ is the shear modulus, $\lambda = 2\nu\mu/(1-2\nu)$ is the Lamé constant, and ν is the Poisson ratio.

One can have the boundary integral equation (BIE) as [37]

$$\mathbf{0} = \int_{\Gamma} \mathbf{U}(\mathbf{x},\mathbf{y})\mathbf{t}(\mathbf{y})\mathrm{d}\Gamma(\mathbf{y}) - \int_{\Gamma} \mathbf{T}(\mathbf{x},\mathbf{y})[\mathbf{u}(\mathbf{y}) - \mathbf{u}(\mathbf{x})]\mathrm{d}\Gamma(\mathbf{y}) \tag{5}$$

where Γ is the boundary of a bounded domain Ω in $\mathbb{R}^2$. $\mathbf{t}$ represents the traction vector on Γ. For plane strain state, the components of $\mathbf{U}(\mathbf{x},\mathbf{y})$ and $\mathbf{T}(\mathbf{x},\mathbf{y})$ are

$$U_{ki}(\mathbf{x},\mathbf{y}) = \frac{-1}{8\pi(1-\nu)\mu}\{(3-4\nu)\ln(r)\delta_{ki} - r_{,k}r_{,i}\} \tag{6}$$

$$T_{ki}(\mathbf{x},\mathbf{y}) = \frac{-1}{4\pi(1-\nu)r}\{[(1-2\nu)\delta_{ki} + 2r_{,k}r_{,i}]\frac{\partial r}{\partial n} - (1-2\nu)(r_{,k}n_i - r_{,i}n_k)\} \tag{7}$$

where $r = \|\mathbf{x}-\mathbf{y}\|$, and $\mathbf{n}(\mathbf{y})$ is the unit outward normal. Points $\mathbf{x}$ and $\mathbf{y}$ are the source point and field point in $\mathbb{R}^2$, respectively.

In conventional BEM or BNM, the boundary Γ in Eq. (5) is approximated by the discrete cells. In BNM, the cells are used for the convenience of computing the integrals on the boundary. In BEM, the cells are also used for approximating the fields and they are called elements. In general, the straight line or the parabola can be used as each cell to approximate the boundary. However, for complex curves, these kinds of cells cannot reproduce the geometries exactly and the discretization error occurs.

In most of the CAD/CAE packages, the curves are represented by parametric functions and only the local coordinates in one-dimensional parameter space are needed to obtain the global coordinates in two-dimensional space. In general, a curve can be represented by parametric functions by

$$x_1 = f_1(\xi); \quad x_2 = f_2(\xi) \tag{8}$$

where $\mathbf{x}\{x_1, x_2\}$ are the global coordinates and ξ is the parameter coordinate. Usually one can use $\mathbf{x}(\xi)$ to clarify that point $\mathbf{x}$ is represented by the parameter ξ in parametric form.

The normal $\mathbf{n}$ of a point $\mathbf{x}$ on the curve can be obtained by

$$\mathbf{n}\{n_1, n_2\} = \{\frac{\partial x_2}{\partial \xi}, -\frac{\partial x_1}{\partial \xi}\} \tag{9}$$

Now suppose the boundary Γ can be represented in parametric form and one can partition it as

$$\Gamma = \sum_{j=1}^{N} \Gamma_j[\xi_j, \xi_{j+1}] \tag{10}$$

where $\Gamma_j[\xi_j, \xi_{j+1}]$ is the jth cell with range $[\xi_j, \xi_{j+1}]$, ξ_j is the jth parameter and N is the number of cells. Γ_j is also represented in parametric form by Eq. (8), thus, the boundary Γ can be reconstituted exactly no matter how many cells are used. This is why the cells are called as isogeometric cells.

Then Eq. (5) can be written as

$$\begin{aligned} &\sum_{j=1}^{N} \int_{\Gamma_j} \mathbf{U}(\mathbf{x}(\varsigma), \mathbf{y}(\xi))\mathbf{t}(\mathbf{y}(\xi))J\mathrm{d}\xi \\ &= \sum_{j=1}^{N} \int_{\Gamma_j} \mathbf{T}(\mathbf{x}(\varsigma), \mathbf{y}(\xi))[\mathbf{u}(\mathbf{y}(\xi)) - \mathbf{u}(\mathbf{x}(\varsigma))]J\mathrm{d}\xi \end{aligned} \tag{11}$$

where ς and ξ are parameter coordinates for points $\mathbf{x}$ and $\mathbf{y}$, respectively. J can be evaluated by

$$J = \sqrt{(\frac{\partial y_1}{\partial \xi})^2 + (\frac{\partial y_2}{\partial \xi})^2} \tag{12}$$

Eq. (11) has partitioned the boundary with isogeometric cells for the purpose of integration. The rest of the problem is how to approximate the field and two methods will be introduced in the next two sections.

3 The Interpolating Isogeometric Boundary Node Method

In this section, the IIMLS method is implemented to obtain the shape function for field approximation and the interpolating isogeometric boundary node method (IIBNM) is derived.

3.1 The Improved Interpolating Moving Least-Square Method [21,31]

Suppose point $\mathbf{x}\{x_1, \ldots, x_d\}$ is a point in a domain Ω in space $\mathbb{R}^d (d = 1, 2, 3)$ and the local support domain $R(\mathbf{x})$ is centered at $\mathbf{x}$. For function $u(\mathbf{x})$, one can define another formula as

$$\tilde{u}(\mathbf{x}, \mathbf{y}) = u(\mathbf{y}) - \sum_{k=1}^{n} q(\mathbf{x}, \mathbf{y}_k) u(\mathbf{y}_k) \tag{13}$$

where $q(\mathbf{x}, \mathbf{y}_i)$ is defined as

$$q(\mathbf{x}, \mathbf{y}_i) = \frac{\zeta(\mathbf{x}, \mathbf{y}_i)}{\sum_{k=1}^{n} \zeta(\mathbf{x}, \mathbf{y}_k)} \tag{14}$$

with

$$\zeta(\mathbf{x}, \mathbf{y}_k) = \frac{\prod_{i=1, i \neq k}^{n} \left\| \mathbf{x} - \mathbf{y}_i \right\|^2}{\prod_{i=1, i \neq k}^{n} \left\| \mathbf{y}_k - \mathbf{y}_i \right\|^2} \tag{15}$$

The function $q(\mathbf{x}, \mathbf{y}_i)$ has the following properties:

$$q(\mathbf{y}_i, \mathbf{y}_j) = \delta_{ij} = \begin{cases} 1, & i = j \\ 0, & i \neq j \end{cases} \tag{16}$$

and

$$\sum_{i=1}^{n} q(\mathbf{x}, \mathbf{y}_i) = 1, \quad \mathbf{x} \in \Omega \tag{17}$$

The local function of $\tilde{u}(\mathbf{x}, \mathbf{y})$ can be evaluated by

$$\tilde{u}^h(\mathbf{x}, \mathbf{y}) = \sum_{j=1}^{m} g_j(\mathbf{x}, \mathbf{y}) a_j(\mathbf{x}) \tag{18}$$

where $a_j(\mathbf{x})$ are coefficients needed to be determined. $g_j(\mathbf{x}, \mathbf{y})$ is defined as

$$g_j(\mathbf{x}, \mathbf{y}) = p_j(\mathbf{y}) - \sum_{i=1}^{n} q(\mathbf{x}, \mathbf{y}_i) p_j(\mathbf{y}_i) \tag{19}$$

In Eq. (19), $p_j(\mathbf{x})$ are basis functions.

To obtain the unknown $a_j(\mathbf{x})$, one can define the weighted discrete L^2 norm as

$$\begin{aligned} J &= \sum_{i=1}^{n} w(\mathbf{x}-\mathbf{y}_i)[\tilde{u}^h(\mathbf{x},\mathbf{y}_i)-\tilde{u}(\mathbf{x},\mathbf{y}_i)]^2 \\ &= \sum_{i=1}^{n} w(\mathbf{x}-\mathbf{y}_i)[\sum_{j=1}^{m} g_j(\mathbf{x},\mathbf{y}_i)a_j(\mathbf{x})-u(\mathbf{y}_i)+\sum_{k=1}^{n} q(\mathbf{x},\mathbf{y}_k)u(\mathbf{y}_k)]^2 \end{aligned} \tag{20}$$

where $w(\mathbf{x}-\mathbf{y}_i)$ are weight functions.

From Eq. (20), we can have

$$\mathbf{A}(\mathbf{x})\mathbf{a}(\mathbf{x}) = \mathbf{B}(\mathbf{x})\mathbf{u} \tag{21}$$

where

$$A_{lj}(\mathbf{x}) = \sum_{i=1}^{n} w(\mathbf{x}-\mathbf{y}_i)g_j(\mathbf{x},\mathbf{y}_i)g_l(\mathbf{x},\mathbf{y}_i) \tag{22}$$

$$B_{lk}(\mathbf{x}) = \sum_{i=1}^{n} w(\mathbf{x}-\mathbf{y}_i)g_l(\mathbf{x},\mathbf{y}_i)[\delta_{ik}-q(\mathbf{x},\mathbf{y}_k)] \tag{23}$$

$$\mathbf{u} = [\,u(\mathbf{y}_1),\quad u(\mathbf{y}_2),\quad \ldots,\quad u(\mathbf{y}_n)\,]^{\mathrm{T}} \tag{24}$$

$$\mathbf{a}(\mathbf{x}) = [\,a_2(\mathbf{x}),\quad a_3(\mathbf{x}),\quad \ldots,\quad a_m(\mathbf{x})\,]^{\mathrm{T}} \tag{25}$$

And

$$\mathbf{a}(\mathbf{x}) = \mathbf{A}^{-1}(\mathbf{x})\mathbf{B}(\mathbf{x})\mathbf{u} \tag{26}$$

Then $\tilde{u}(\mathbf{x},\mathbf{y})$ will be expressed as

$$\tilde{u}^h(\mathbf{x},\mathbf{y}) = \hat{\mathbf{g}}(\mathbf{x},\mathbf{y})\mathbf{A}^{-1}(\mathbf{x})\mathbf{B}(\mathbf{x})\mathbf{u} \tag{27}$$

With

$$\hat{\mathbf{g}}(\mathbf{x},\mathbf{y}) = [g_2(\mathbf{x},\mathbf{y}), g_3(\mathbf{x},\mathbf{y}), \ldots, g_m(\mathbf{x},\mathbf{y})] \tag{28}$$

Finally, if letting $\mathbf{y}=\mathbf{x}$, we can evaluate $u(\mathbf{x})$ by

$$u(\mathbf{x}) = \hat{\mathbf{g}}(\mathbf{x},\mathbf{x})\mathbf{A}^{-1}(\mathbf{x})\mathbf{B}(\mathbf{x})\mathbf{u} + \mathbf{q}(\mathbf{x})\mathbf{u} = \mathbf{\Phi}(\mathbf{x})\mathbf{u} \tag{29}$$

where

$$\mathbf{\Phi}(\mathbf{x}) = \hat{\mathbf{g}}(\mathbf{x},\mathbf{x})\mathbf{A}^{-1}(\mathbf{x})\mathbf{B}(\mathbf{x}) + \mathbf{q}(\mathbf{x}) \tag{30}$$

$$\mathbf{q}(\mathbf{x}) = [\,q(\mathbf{x},\mathbf{y}_1),\quad q(\mathbf{x},\mathbf{y}_2),\quad \ldots,\quad q(\mathbf{x},\mathbf{y}_n)\,] \tag{31}$$

And shape functions $\mathbf{\Phi}(\mathbf{x})$ have [32]:

Property 1. Interpolating property:

$$\Phi_i(\mathbf{x}_j) = \delta_{ij} = \begin{cases} 1, & i = j \\ 0, & i \neq j \end{cases} \tag{32}$$

Property 2. Reproducing property:

$$\sum_{i=1}^{n} \Phi_i(\mathbf{x}) p_j(\mathbf{y}_i) = p_j(\mathbf{x}) \tag{33}$$

3.2 The Interpolating Isogeometric Boundary Node Method

With the IIMLS approximation, a meshless interpolating isogeometric boundary node method (IIMLS) can be obtained. The displacements $\mathbf{u}(\mathbf{y})$ and tractions $\mathbf{t}(\mathbf{y})$ on the boundary point $\mathbf{y}$ can be interpolated by

$$u_l(\mathbf{y}) = u_l(\mathbf{y}(\xi)) = \sum_{i=1}^{n} \Phi_i(\xi) u_l^i = \mathbf{\Phi}(\xi)\mathbf{u}_l \tag{34}$$

$$t_l(\mathbf{y}) = t_l(\mathbf{y}(\xi)) = \sum_{i=1}^{n} \Phi_i(\xi) t_l^i = \mathbf{\Phi}(\xi)\mathbf{t}_l \tag{35}$$

where ξ is the parameter coordinate for point $\mathbf{y}$, u_l^i and t_l^i are the nodal displacement and traction, and $\Phi_i(\xi)$ is the shape function obtained by IIMLS method as

$$\mathbf{\Phi}(\xi) = \hat{\mathbf{g}}(\xi, \xi)\mathbf{A}^{-1}(\xi)\mathbf{B}(\xi) + \mathbf{q}(\xi) \tag{36}$$

By substituting Eqs. (34) and (35) into Eq. (11), one can obtain

$$\begin{aligned} &\sum_{j=1}^{N} \int_{\Gamma_j} U_{kl}(\mathbf{x}(\varsigma), \mathbf{y}(\xi)) \sum_{i=1}^{n} \Phi_i(\xi) t_l^i J \mathrm{d}\xi \\ &= \sum_{j=1}^{N} \int_{\Gamma_j} T_{kl}(\mathbf{x}(\varsigma), \mathbf{y}(\xi)) [\sum_{i=1}^{n} \Phi_i(\xi) u_l^i - \sum_{i=1}^{n} \Phi_i(\varsigma) u_l^i] J \mathrm{d}\xi \end{aligned} \tag{37}$$

For boundary node $x(\xi_p)$, Eq. (37) can be rewritten as:

$$\begin{aligned} &\sum_{j=1}^{N} \int_{\Gamma_j} U_{kl}(\mathbf{x}(\xi_p), \mathbf{y}(\xi)) \sum_{i=1}^{n} \Phi_i(\xi) t_l^i J \mathrm{d}\xi \\ &= \sum_{j=1}^{N} \int_{\Gamma_j} T_{kl}(\mathbf{x}(\xi_p), \mathbf{y}(\xi)) [\sum_{i=1}^{n} \Phi_i(\xi) u_l^i] J \mathrm{d}\xi \\ &- \sum_{j=1}^{N} \int_{\Gamma_j} T_{kl}(\mathbf{x}(\xi_p), \mathbf{y}(\xi)) u_l^p J \mathrm{d}\xi \end{aligned} \tag{38}$$

Finally, Eq. (38) can be rewritten as

$$\mathbf{Hu} = \mathbf{Gt} \tag{39}$$

where

$$\begin{aligned}\left[H_{pi}\right] &= \sum_{\Gamma_j \in \mathrm{K}_i} \int_{\Gamma_j} \begin{bmatrix} T_{11}(\mathbf{x}(\xi_p), \mathbf{y}(\xi)) & T_{12}(\mathbf{x}(\xi_p), \mathbf{y}(\xi)) \\ T_{21}(\mathbf{x}(\xi_p), \mathbf{y}(\xi)) & T_{22}(\mathbf{x}(\xi_p), \mathbf{y}(\xi)) \end{bmatrix} \Phi_i(\xi) J \mathrm{d}\xi \\ &- \delta_{pi} \sum_{\Gamma_j \in \mathrm{K}_p} \int_{\Gamma_j} \begin{bmatrix} T_{11}(\mathbf{x}(\xi_p), \mathbf{y}(\xi)) & T_{12}(\mathbf{x}(\xi_p), \mathbf{y}(\xi)) \\ T_{21}(\mathbf{x}(\xi_p), \mathbf{y}(\xi)) & T_{22}(\mathbf{x}(\xi_p), \mathbf{y}(\xi)) \end{bmatrix} J \mathrm{d}\xi \end{aligned} \tag{40}$$

$$\left[G_{pi}\right] = \sum_{\Gamma_j \in \mathrm{K}_i} \int_{\Gamma_j} \begin{bmatrix} U_{11}(\mathbf{x}(\xi_p), \mathbf{y}(\xi)) & U_{12}(\mathbf{x}(\xi_p), \mathbf{y}(\xi)) \\ U_{21}(\mathbf{x}(\xi_p), \mathbf{y}(\xi)) & U_{22}(\mathbf{x}(\xi_p), \mathbf{y}(\xi)) \end{bmatrix} \Phi_i(\xi) J \mathrm{d}\xi \tag{41}$$

$$\mathbf{u} = \begin{bmatrix} u_1^1 & u_2^1 & \cdots & u_1^n & u_2^n \end{bmatrix}^{\mathrm{T}} \tag{42}$$

$$\mathbf{t} = \begin{bmatrix} t_1^1 & t_2^1 & \cdots & t_1^n & t_2^n \end{bmatrix}^{\mathrm{T}} \tag{43}$$

In Eqs. (40) and (41), K_i is the set of cells that have contributions to $\Phi_i(\xi)$ and K_p is the set of cells contain node $\mathbf{x}(\xi_p)$ (see Fig. 1).

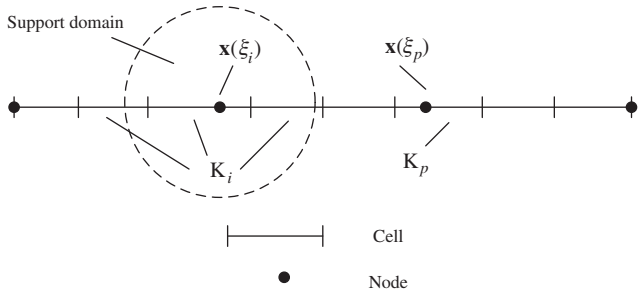

Figure 1: Cells and nodes in IIBNM

4 The Isogeometric Boundary Element Method

In IIBNM, the integral cells and field approximations are independent. In this section, the isogeometric cells are also used to interpolate the fields and the shape functions used in traditional BEM are applied. The method can also be called an isogeometric boundary element method (IBEM). The interpolation is also performed in parameter space and a coordinate transformation is defined in a cell $\Gamma_j[\xi_j, \xi_{j+1}]$ as

$$\xi(s) = \frac{\xi_{j+1} - \xi_j}{2} s + \frac{\xi_{j+1} + \xi_j}{2} \tag{44}$$

where $s \in [-1, 1]$ is the local coordinate (see Fig. 2). If the values at nodes ξ_j and ξ_{j+1} are used to interpolate the field in the cell $\Gamma_j[\xi_j, \xi_{j+1}]$, then $\mathbf{u}(\mathbf{y})$ and $\mathbf{t}(\mathbf{y})$ at point $\mathbf{y} \in \Gamma_j$ can be interpolated by

$$u_l(\mathbf{y}) = u_l(\mathbf{y}(\xi(s))) = \sum_{i=0}^{1} \psi_j^i(s) u_l^{i+j} \tag{45}$$

$$t_l(\mathbf{y}) = t_l(\mathbf{y}(\xi(s))) = \sum_{i=0}^{1} \psi_j^i(s) t_l^{i+j} \tag{46}$$

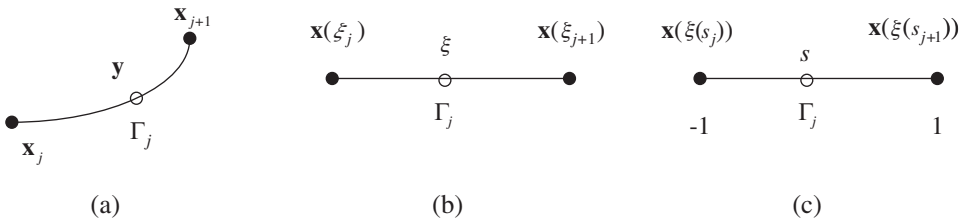

Figure 2: Local coordinate. (a) global space. (b) parameter space. (c) local coordinate

where $\mathbf{u}^j$ and $\mathbf{t}^j$ are the displacements and tractions at point $\mathbf{x}_j$, and $\psi_j^i(s)$ is the shape function on Γ_j defined as

$$\psi_j^0(s) = 0.5 - 0.5s \tag{47}$$

$$\psi_j^1(s) = 0.5 + 0.5s \tag{48}$$

By substituting Eqs. (45) and (46) into Eq. (11), one can obtain

$$\begin{aligned}&\sum_{j=1}^{N}\int_{\Gamma_j} U_{kl}(\mathbf{x}(\varsigma(q)),\mathbf{y}(\xi(s)))\sum_{i=0}^{1}\psi_j^i(s)t_l^{i+j}JJ_1\mathrm{d}s\\&=\sum_{j=1}^{N}\int_{\Gamma_j} T_{kl}(\mathbf{x}(\varsigma(q)),\mathbf{y}(\xi(s)))[\sum_{i=0}^{1}\psi_j^i(s)u_l^{i+j}-\sum_{i=0}^{1}\psi_j^i(q)t_l^{i+j}]JJ_1\mathrm{d}s\end{aligned} \tag{49}$$

where q is the new local coordinate of ς in the relative cell and $J_1 = (\xi_{j+1} - \xi_j)/2$. Then for $\mathbf{x}(\xi(s_p))$, we can have:

$$\begin{aligned}&\sum_{j=1}^{N}\int_{\Gamma_j} U_{kl}(\mathbf{x}(\xi(s_p)),\mathbf{y}(\xi(s)))\sum_{i=0}^{1}\psi_j^i(s)t_l^{i+j}JJ_1\mathrm{d}s\\&=\sum_{j=1}^{N}\int_{\Gamma_j} T_{kl}(\mathbf{x}(\xi(s_p)),\mathbf{y}(\xi(s)))[\sum_{i=0}^{1}\psi_j^i(s)u_l^{i+j}-\sum_{i=0}^{1}\psi_j^i(s_p)t_l^{i+j}]JJ_1\mathrm{d}s\end{aligned} \tag{50}$$

The shape function in Eq. (50) also has the interpolating property, thus, one can obtain

$$\begin{aligned}&\sum_{j=1}^{N}\int_{\Gamma_j} U_{kl}(\mathbf{x}(\xi(s_p)),\mathbf{y}(\xi(s)))\sum_{i=0}^{1}\psi_j^i(s)t_l^{i+j}JJ_1\mathrm{d}s\\&=\sum_{j=1}^{N}\int_{\Gamma_j} T_{kl}(\mathbf{x}(\xi(s_p)),\mathbf{y}(\xi(s)))\sum_{i=0}^{1}\psi_j^i(s)u_l^{i+j}JJ_1\mathrm{d}s\\&-\sum_{j=1}^{N}\int_{\Gamma_j} T_{kl}(\mathbf{x}(\xi(s_p)),\mathbf{y}(\xi(s)))t_l^{p+j}JJ_1\mathrm{d}s\end{aligned} \tag{51}$$

Finally, Eq. (51) will be

$$\mathbf{Hu} = \mathbf{Gt} \tag{52}$$

where

$$\begin{aligned}[H_{pi}] = &\sum_{\Gamma_j \in \mathrm{K}_i} \int_{\Gamma_j} \begin{bmatrix} T_{11}(\mathbf{x}(\xi(s_p)), \mathbf{y}(\xi(s))) & T_{12}(\mathbf{x}(\xi(s_p)), \mathbf{y}(\xi(s))) \\ T_{21}(\mathbf{x}(\xi(s_p)), \mathbf{y}(\xi(s))) & T_{22}(\mathbf{x}(\xi(s_p)), \mathbf{y}(\xi(s))) \end{bmatrix} \psi_j^i(s) JJ_1 \mathrm{d}s \\ &- \delta_{pi} \sum_{\Gamma_j \in \mathrm{K}_p} \int_{\Gamma_j} \begin{bmatrix} T_{11}(\mathbf{x}(\xi(s_p)), \mathbf{y}(\xi(s))) & T_{12}(\mathbf{x}(\xi(s_p)), \mathbf{y}(\xi(s))) \\ T_{21}(\mathbf{x}(\xi(s_p)), \mathbf{y}(\xi(s))) & T_{22}(\mathbf{x}(\xi(s_p)), \mathbf{y}(\xi(s))) \end{bmatrix} JJ_1 \mathrm{d}s \end{aligned} \tag{53}$$

$$[G_{pi}] = \sum_{\Gamma_j \in \mathrm{K}_i} \int_{\Gamma_j} \begin{bmatrix} U_{11}(\mathbf{x}(\xi(s_p)), \mathbf{y}(\xi(s))) & U_{12}(\mathbf{x}(\xi(s_p)), \mathbf{y}(\xi(s))) \\ U_{21}(\mathbf{x}(\xi(s_p)), \mathbf{y}(\xi(s))) & U_{22}(\mathbf{x}(\xi(s_p)), \mathbf{y}(\xi(s))) \end{bmatrix} \psi_j^i(s) JJ_1 \mathrm{d}s \tag{54}$$

In Eqs. (53) and (54), K_i are cells cover node $\mathbf{x}(\xi(s_i))$ (see Fig. 3).

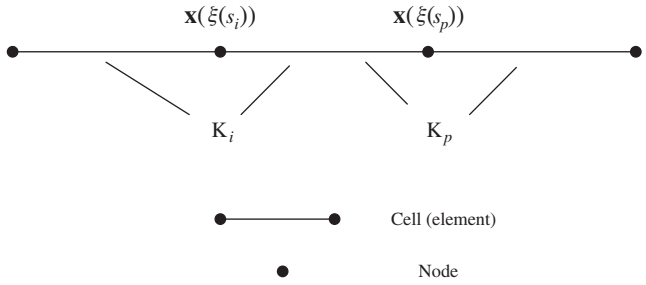

Figure 3: Cells and nodes in IBEM

5 Numerical Examples

In all the examples, $E = 2.5$ and $v = 0.3$ are applied for the material properties. To treat the singular integrals appeared in the proposed methods, the rigid body motion method is applied to compute the strongly singular integrals, and the self-adaptive coordinate transformation method [38] is used to evaluate the weakly singular integrals [37].

5.1 Dirichlet Problems on a Ring

A ring shown in Fig. 4 is tested in this example. The radius of the inner circle is 1, and the minimum radius and maximum radius of the outer ellipse are 2 and 4, respectively. Displacements are known on all the boundaries and the following solutions are considered:

(i) Linear solution:

$$u_1 = 2x_1 + 3x_2 \tag{55}$$

$$u_2 = 3x_1 + 2x_2 \tag{56}$$

(ii) Quadratic solution:

$$u_1 = x_2^2 - 2x_1x_2 - x_1^2 \tag{57}$$

$$u_2 = x_2^2 + 2x_1x_2 - x_1^2 \tag{58}$$

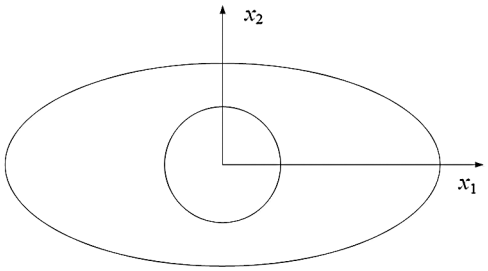

Figure 4: A ring

(iii) Cubic solution:

$$u_1 = x_2^3 - 3x_1^2 x_2 \tag{59}$$

$$u_2 = -x_1^3 + 3x_2^2 x_1 \tag{60}$$

The relative errors of the displacements and stresses are shown in Figs. 5–7. One can indicate that both IIBNM and IBEM have good agreement with the exact results. The errors of IIBNM and IBEM are very close to each other for the cases with few nodes. It can also be observed that the results obtained by IIBNM have a little concussion when the boundary nodes are few.

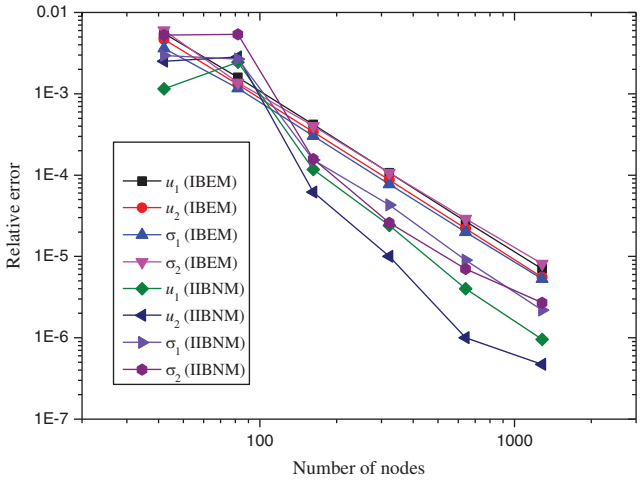

Figure 5: Relative errors for linear solution

5.2 Lame Problem

The Lame problem shown in Fig. 8 is considered. Plane strain state is considered and geometry shown in Fig. 8(b) is analyzed.

The exact solutions for this problem are

$$\sigma_r = \frac{a^2 p}{b^2 - a^2}\left(1 - \frac{b^2}{r^2}\right) \tag{61}$$

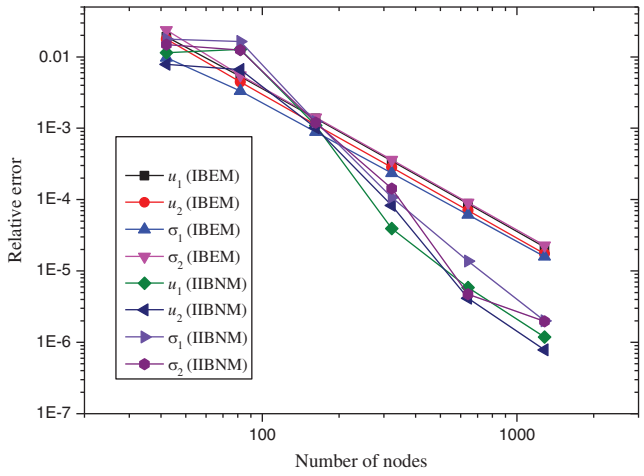

Figure 6: Relative errors for quadratic solution

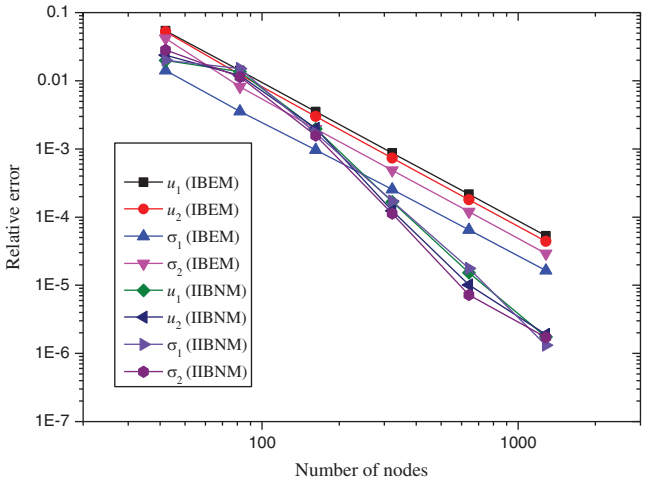

Figure 7: Relative errors for cubic solution

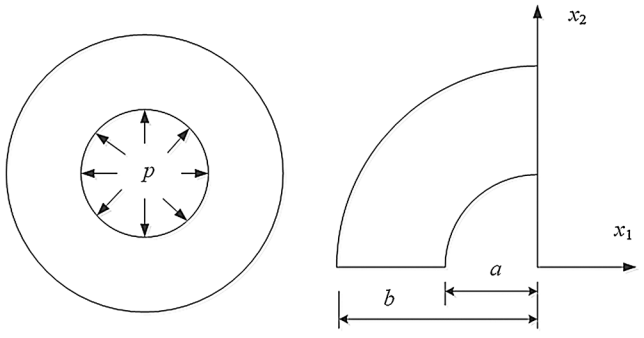

Figure 8: Lame problem

$$\sigma_\theta = \frac{a^2 p}{b^2 - a^2}(1 + \frac{b^2}{r^2}) \tag{62}$$

$a = 1$, $b = 2$ and $p = 1$ are implemented. The results of traction t_2 on line $x_2 = 0$ are plotted in Fig. 9. All the results shown in Fig. 9 are solved by 69 boundary nodes. Fig. 10 shows the relative errors of traction t_2 on line $x_2 = 0$ for different methods. It can be observed that the accuracy of IIBNM is the highest.

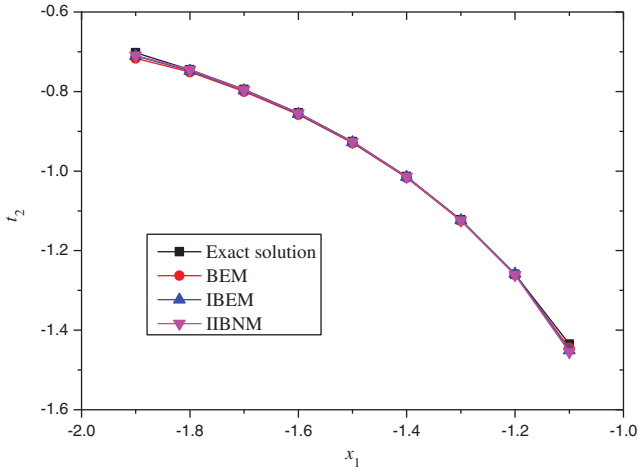

Figure 9: Results of traction

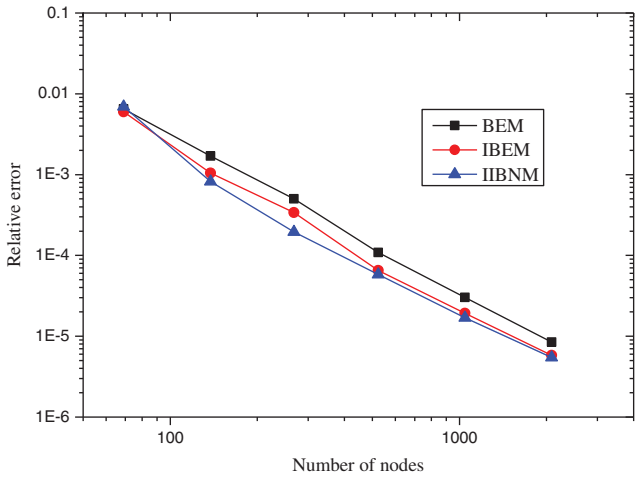

Figure 10: Relative error of the traction

5.3 Plate with an Elliptical Hole

In this example, a geometry under tensile load shown in Fig. 11 is studied and the parameters are $L = 20$, $r_1 = 2, r_2 = 4$ and $T = 1$. Plane stress statement is assumed. 3845 nodes are used in IBEM and IIBNM while 344363 CPS4R elements are used in FEM to solve the problem.

The stresses σ_2 on line $x_2 = 0$ are shown in Fig. 12 and the stresses σ_1 on line $x_1 = 0$ are shown in Fig. 13. One can find out that similar results are obtained by the proposed methods, compared with FEM.

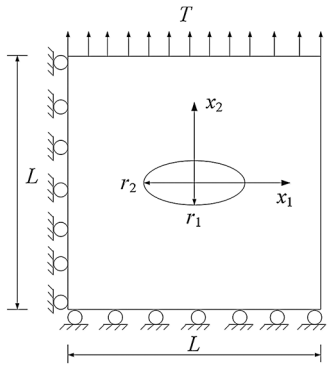

Figure 11: A plate with an elliptical hole

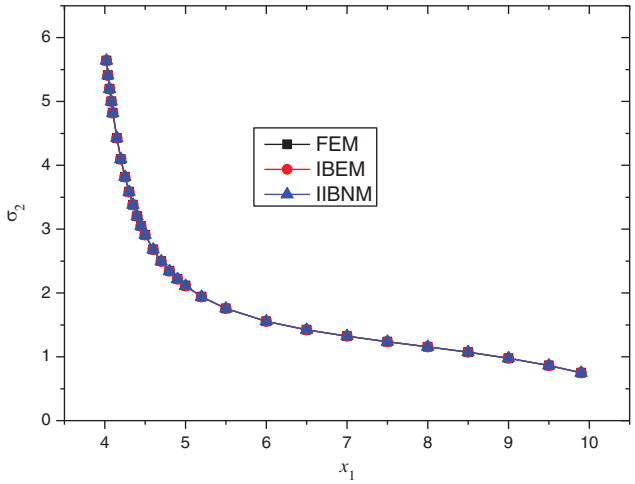

Figure 12: Stresses on line $x_2 = 0$

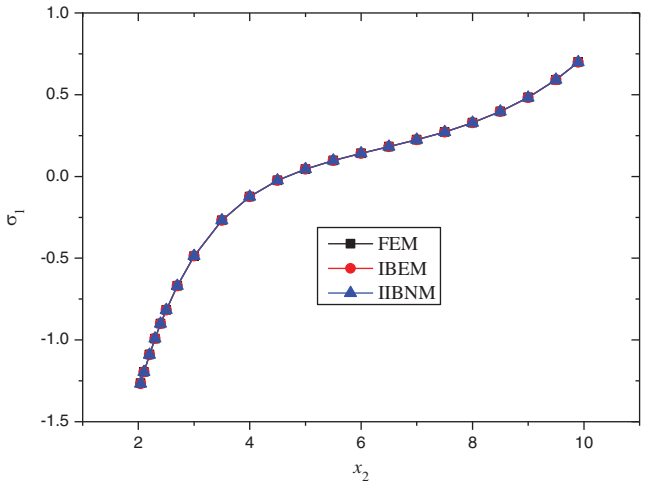

Figure 13: Stresses on line $x_1 = 0$

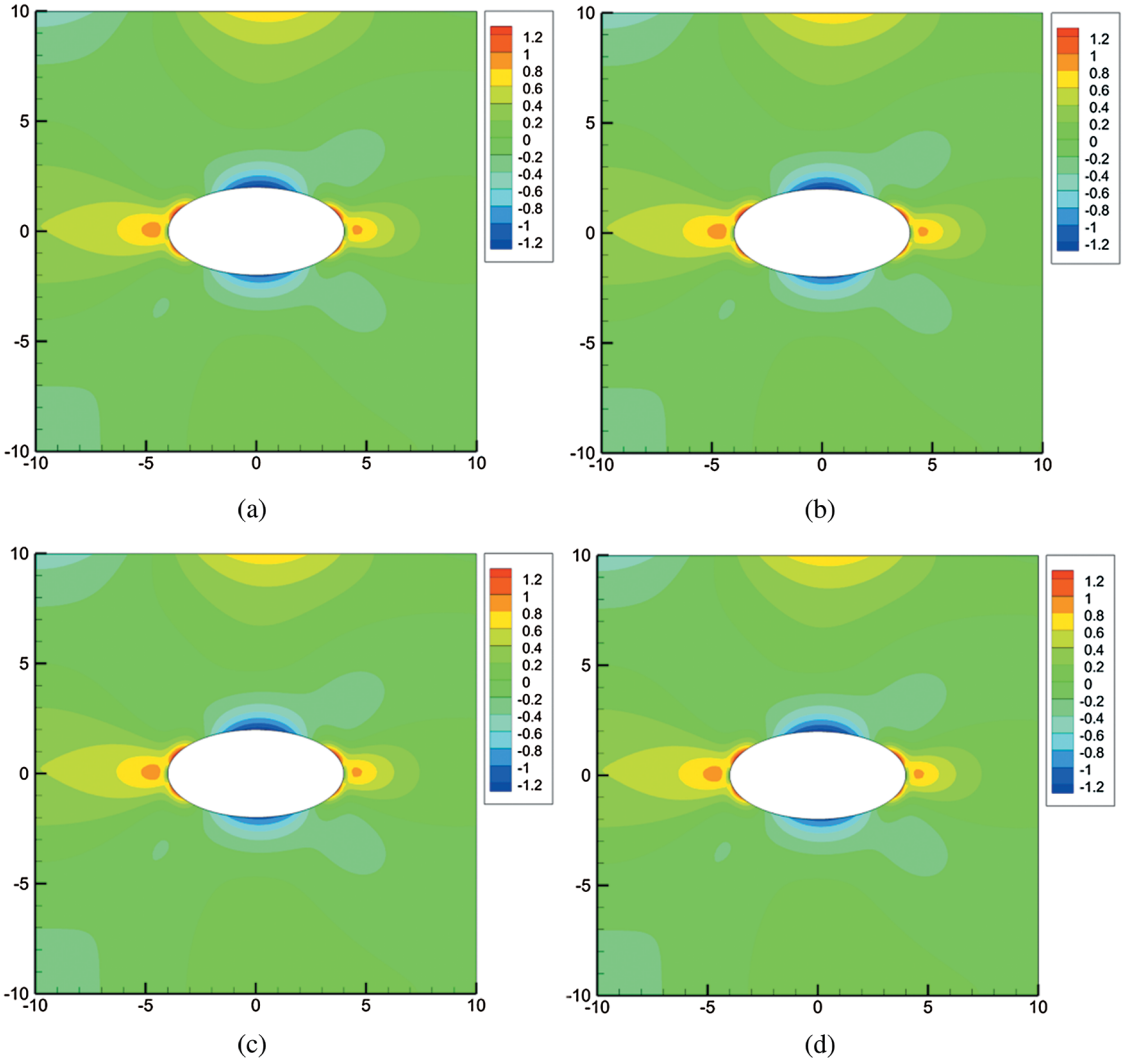

Figure 14: Contours of stress σ_1 for a plate with an elliptical hole. (a) FEM. (b) BEM. (c) IBEM. (d) IIBNM

The contours of stresses σ_1 and σ_2 are shown in Figs. 14 and 15. Conventional BEM with 3845 nodes is also used to simulate the problem. It can be observed that the results obtained by FEM, BEM, IBEM, and IIBNM have little difference.

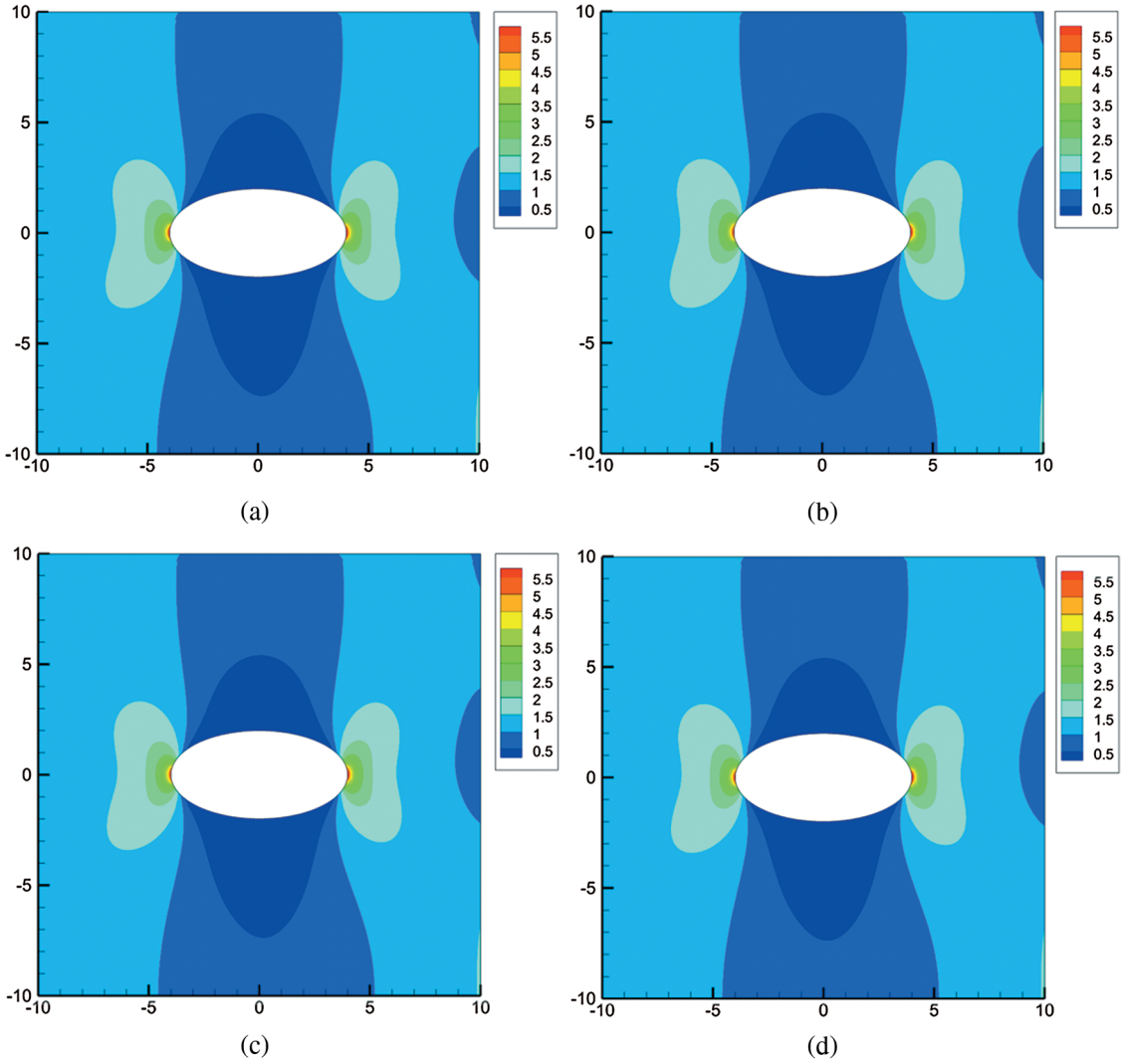

Figure 15: Contours of stress σ_2 for a plate with an elliptical hole. (a) FEM. (b) BEM. (c) IBEM. (d) IIBNM

6 Conclusions

Two general isogeometric methods based on the parameter space are proposed. The integral cells and elements are defined in parameter space, and the geometry can be reproduced at all the stages in both methods. The displacement and traction fields are approximated by the IIMLS method and Lagrangian basis functions in parameter space in IIBNM and IBEM, respectively.

Coupling the methods with the fast multipole method (FMM) [39–41] and domain integration methods [42] for non-homogeneous problems are under research. The proposed methods can also be applied in many other problems, such as fracture problems [43–48].

Funding Statement: The research for this paper was supported by (1) the National Natural Science Foundation of China (Grants Nos. 51708429, 51708428), and (2) the Open Projects Foundation (Grant No. 2017-04-GF) of State Key Laboratory for Health and Safety of Bridge Structures, and (3) Wuhan Institute of Technology Science Found (Grant No. K201734), and (4) the science and technology projects of Wuhan Urban and Rural Construction Bureau (Grants Nos. 201831, 201919).

Conflicts of Interest: The authors declare that they have no conflicts of interest to report regarding the present study.

References

1. Hughes, T. J., Cottrell, J. A., Bazilevs, Y. (2005). Isogeometric analysis: CAD, finite elements, NURBS, exact geometry and mesh refinement. *Computer Methods in Applied Mechanics and Engineering, 194(39),* 4135–4195. DOI 10.1016/j.cma.2004.10.008.
2. Cottrell, J. A., Hughes, T. J., Bazilevs, Y. (2009). *Isogeometric analysis: toward integration of CAD and FEA*. United Kingdom: John Wiley & Sons.
3. Wang, Q., Zhou, W., Cheng, Y., Ma, G., Chang, X. et al. (2018). NE-IIBEFM for problems with body forces: a seamless integration of the boundary type meshfree method and the NURBS boundary in CAD. *Advances in Engineering Software, 118,* 1–17. DOI 10.1016/j.advengsoft.2018.01.002.
4. Yao, Z., Wang, H. (2013). Some benchmark problems and basic ideas on the accuracy of boundary element analysis. *Engineering Analysis with Boundary Elements, 37(12),* 1674–1692. DOI 10.1016/j.enganabound.2013.10.001.
5. Wang, H., Yao, Z. (2005). A new fast multipole boundary element method for large scale analysis of mechanical properties in 3D particle-reinforced composites. *Computer Modeling in Engineering & Sciences, 7(1),* 85–95.
6. Liu, Y. (2006). A new fast multipole boundary element method for solving large-scale two-dimensional elastostatic problems. *International Journal for Numerical Methods in Engineering, 65(6),* 863–881. DOI 10.1002/nme.1474.
7. Wang, Q., Zhou, W., Cheng, Y., Ma, G., Chang, X. (2017). A line integration method for the treatment of 3D domain integrals and accelerated by the fast multipole method in the BEM. *Computational Mechanics, 59(4),* 611–624. DOI 10.1007/s00466-016-1363-2.
8. Wang, Q., Zhou, W., Cheng, Y., Ma, G., Chang, X. et al. (2017). The boundary element method with a fast multipole accelerated integration technique for 3D elastostatic problems with arbitrary body forces. *Journal of Scientific Computing, 71(3),* 1238–1264. DOI 10.1007/s10915-016-0335-1.
9. Yao, Z. (2016). A new type of high-accuracy BEM and local stress analysis of real beam, plate and shell structures. *Engineering Analysis with Boundary Elements, 65,* 1–17. DOI 10.1016/j.enganabound.2015.12.011.
10. Simpson, R. N., Bordas, S. P., Trevelyan, J., Rabczuk, T. (2012). A two-dimensional isogeometric boundary element method for elastostatic analysis. *Computer Methods in Applied Mechanics and Engineering, 209,* 87–100. DOI 10.1016/j.cma.2011.08.008.
11. Gu, J., Zhang, J., Li, G. (2012). Isogeometric analysis in BIE for 3-D potential problem. *Engineering Analysis with Boundary Elements, 36(5),* 858–865. DOI 10.1016/j.enganabound.2011.09.018.
12. Marussig, B., Beer, G., Duenser, C. (2014). Isogeometric boundary element method for the simulation in tunneling. *Applied Mechanics & Materials, 553,* 495–500. DOI 10.4028/www.scientific.net/AMM.553.495.
13. Heltai, L., Arroyo, M., DeSimone, A. (2014). Nonsingular isogeometric boundary element method for Stokes flows in 3D. *Computer Methods in Applied Mechanics and Engineering, 268,* 514–539. DOI 10.1016/j.cma.2013.09.017.
14. Zhang, J., Qin, X., Han, X., Li, G. (2009). A boundary face method for potential problems in three dimensions. *International Journal for Numerical Methods in Engineering, 80(3),* 320–337. DOI 10.1002/nme.2633.
15. Zhou, F., Zhang, J., Sheng, X., Li, G. (2011). Shape variable radial basis function and its application in dual reciprocity boundary face method. *Engineering Analysis with Boundary Elements, 35(2),* 244–252. DOI 10.1016/j.enganabound.2010.08.009.
16. Zhou, F., Zhang, J., Sheng, X., Li, G. (2012). A dual reciprocity boundary face method for 3D non-homogeneous elasticity problems. *Engineering Analysis with Boundary Elements, 36(9),* 1301–1310. DOI 10.1016/j.enganabound.2012.03.009.
17. Zhang, J., Yao, Z., Li, H. (2002). A hybrid boundary node method. *International Journal for Numerical Methods in Engineering, 53(4),* 751–763. DOI 10.1002/nme.313.
18. Miao, Y., He, T., Luo, H., Zhu, H. (2012). Dual hybrid boundary node method for solving transient dynamic fracture problems. *Computer Modeling in Engineering & Sciences, 85(6),* 481–498.

19. Miao, Y., He, T., Yang, Q., Zheng, J. (2010). Multi-domain hybrid boundary node method for evaluating top-down crack in Asphalt pavements. *Engineering Analysis with Boundary Elements, 34(9),* 755–760. DOI 10.1016/j.enganabound.2010.04.002.
20. Miao, Y., Wang, Y., Wang, Y. (2009). A meshless hybrid boundary-node method for Helmholtz problems. *Engineering Analysis with Boundary Elements, 33(2),* 120–127. DOI 10.1016/j.enganabound.2008.05.009.
21. Wang, J., Wang, J., Sun, F., Cheng, Y. (2013). An interpolating boundary element-free method with nonsingular weight function for two-dimensional potential problems. *International Journal of Computational Methods, 10(6),* 1350043. DOI 10.1142/S0219876213500436.
22. Chen, L., Liu, X., Li, X. (2019). The boundary element-free method for 2D interior and exterior Helmholtz problems. *Computers & Mathematics with Applications, 77(3),* 846–864. DOI 10.1016/j.camwa.2018.10.022.
23. Chen, L., Li, X. (2020). A complex variable boundary element-free method for the Helmholtz equation using regularized combined field integral equations. *Applied Mathematics Letters, 101,* 106067. DOI 10.1016/j.aml.2019.106067.
24. Mukherjee, Y. X., Mukherjee, S. (1997). The boundary node method for potential problems. *International Journal for Numerical Methods in Engineering, 40(5),* 797–815.
25. Li, X. (2011). The meshless Galerkin boundary node method for Stokes problems in three dimensions. *International Journal for Numerical Methods in Engineering, 88(5),* 442–472. DOI 10.1002/nme.3181.
26. Li, X., Zhu, J. (2009). A Galerkin boundary node method and its convergence analysis. *Journal of Computational and Applied Mathematics, 230(1),* 314–328. DOI 10.1016/j.cam.2008.12.003.
27. Lancaster, P., Salkauskas, K. (1981). Surfaces generated by moving least squares methods. *Mathematics of Computation, 37(155),* 141–158. DOI 10.1090/S0025-5718-1981-0616367-1.
28. Li, X. (2016). Error estimates for the moving least-square approximation and the element-free Galerkin method in n-dimensional spaces. *Applied Numerical Mathematics, 99,* 77–97. DOI 10.1016/j.apnum.2015.07.006.
29. Li, X., Li, S. (2016). On the stability of the moving least squares approximation and the element-free Galerkin method. *Computers & Mathematics with Applications, 72(6),* 1515–1531. DOI 10.1016/j.camwa.2016.06.047.
30. Liew, K., Cheng, Y., Kitipornchai, S. (2006). Boundary element-free method (BEFM) and its application to two-dimensional elasticity problems. *International Journal for Numerical Methods in Engineering, 65(8),* 1310–1332. DOI 10.1002/nme.1489.
31. Wang, J., Sun, F., Cheng, Y. (2012). An improved interpolating element-free Galerkin method with a nonsingular weight function for two-dimensional potential problems. *Chinese Physics B, 21(9),* 090204. DOI 10.1088/1674-1056/21/9/090204.
32. Li, X. (2015). An interpolating boundary element-free method for three-dimensional potential problems. *Applied Mathematical Modelling, 39(10–11),* 3116–3134. DOI 10.1016/j.apm.2014.10.071.
33. Wang, Q., Zhou, W., Cheng, Y., Ma, G., Chang, X. et al. (2018). Regularized moving least-square method and regularized improved interpolating moving least-square method with nonsingular moment matrices. *Applied Mathematics and Computation, 325,* 120–145. DOI 10.1016/j.amc.2017.12.017.
34. Wang, Q., Zhou, W., Feng, Y. T., Ma, G., Cheng, Y. et al. (2019). An adaptive orthogonal improved interpolating moving least-square method and a new boundary element-free method. *Applied Mathematics and Computation, 353,* 347–370. DOI 10.1016/j.amc.2019.02.013.
35. Simpson, R. N., Bordas, S. P. A., Lian, H., Trevelyan, J. (2013). An isogeometric boundary element method for elastostatic analysis: 2D implementation aspects. *Computers & Structures, 118,* 2–12. DOI 10.1016/j.compstruc.2012.12.021.
36. Scott, M. A., Simpson, R. N., Evans, J. A., Lipton, S., Bordas, S. P. et al. (2013). Isogeometric boundary element analysis using unstructured T-splines. *Computer Methods in Applied Mechanics and Engineering, 254,* 197–221. DOI 10.1016/j.cma.2012.11.001.
37. Wang, Q., Zhou, W., Cheng, Y., Ma, G., Chang, X. (2019). NURBS-enhanced line integration boundary element method for 2D elasticity problems with body forces. *Computers & Mathematics with Applications, 77(7),* 2006–2028. DOI 10.1016/j.camwa.2018.11.039.

38. Telles, J. (1987). A self-adaptive co-ordinate transformation for efficient numerical evaluation of general boundary element integrals. *International Journal for Numerical Methods in Engineering, 24(5),* 959–973. DOI 10.1002/nme.1620240509.

39. Wang, Q., Miao, Y., Zhu, H. (2013). A fast multipole hybrid boundary node method for composite materials. *Computational Mechanics, 51(6),* 885–897. DOI 10.1007/s00466-012-0766-y.

40. Wang, Q., Zhou, W., Cheng, Y., Ma, G., Chang, X. et al. (2017). An adaptive cell-based domain integration method for treatment of domain integrals in 3D boundary element method for potential and elasticity problems. *Acta Mechanica Solida Sinica, 30(1),* 99–111. DOI 10.1016/j.camss.2016.08.002.

41. Wang, Q., Zhou, W., Cheng, Y., Ma, G., Chang, X. (2017). Fast multipole cell-based domain integration method for treatment of volume potentials in 3D elasticity problems. *Engineering Computations, 34(6),* 1849–1873. DOI 10.1108/EC-03-2016-0111.

42. Zhou, W., Wang, Q., Cheng, Y., Ma, G. (2016). A fast multipole method accelerated adaptive background cell-based domain integration method for evaluation of domain integrals in 3D boundary element method. *Engineering Analysis with Boundary Elements, 67,* 1–12. DOI 10.1016/j.enganabound.2016.03.002.

43. Yan, F., Feng, X., Lv, J., Pan, P., Li, S. (2018). Continuous-discontinuous cellular automaton method for cohesive crack growth in rock. *Engineering Fracture Mechanics, 188,* 361–380. DOI 10.1016/j.engfracmech.2017.09.007.

44. Yan, F., Pan, P., Feng, X., Li, S. (2018). The continuous-discontinuous cellular automaton method for elastodynamic crack problems. *Engineering Fracture Mechanics, 204,* 482–496. DOI 10.1016/j.engfracmech.2018.10.025.

45. Feng, S. Z., Han, X. (2019). A novel multi-grid based reanalysis approach for efficient prediction of fatigue crack propagation. *Computer Methods in Applied Mechanics and Engineering, 353,* 107–122. DOI 10.1016/j.cma.2019.05.001.

46. Zhou, W., Liu, B., Wang, Q., Chang, X., Chen, X. (2020). Formulations of displacement discontinuity method for crack problems based on boundary element method. *Engineering Analysis with Boundary Elements, 115,* 86–95. DOI 10.1016/j.enganabound.2020.03.007.

47. Wang, Q., Zhou, W., Feng, Y. T. (2020). The phase-field model with an auto-calibrated degradation function based on general softening laws for cohesive fracture. *Applied Mathematical Modelling, 86,* 185–206. DOI 10.1016/j.apm.2020.05.005.

48. Wang, Q., Feng, Y. T., Zhou, W., Cheng, Y., Ma, G. (2020). A phase-field model for mixed-mode fracture based on a unified tensile fracture criterion. *Computer Methods in Applied Mechanics and Engineering, 370,* 113270. DOI 10.1016/j.cma.2020.113270.